Cationic Gemini Surfactant-Assisted Synthesis of Hollow Au Nanostructures by Stepwise Reductions

Wentao Wang, Yuchun Han, Maozhang Tian, Yaxun Fan, Yongqiang Tang, Mingyuan Gao,* and Yilin Wang*

Key Laboratory of Colloid and Interface Science, Beijing National Laboratory for Molecular Sciences (BNLMS), Institute of Chemistry, Chinese Academy of Sciences, Beijing 100190, People's Republic of China

Ⓢ Supporting Information

ABSTRACT: A novel synthetic approach was developed for creating versatile hollow Au nanostructures by stepwise reductions of Au^{III} upon the use of cationic gemini surfactant hexamethylene-1,6-bis(dodecyl dimethylammonium bromide) ($C_{12}C_6C_{12}Br_2$) as a template agent. It was observed that the Au^{I} ions obtained from the reduction of Au^{III} by ascorbic acid can assist the gemini surfactant to form vesicles, capsule-like, and tube-like aggregates that subsequently act as soft templates for hollow Au nanostructures upon further reduction of Au^{I} to Au^{0} by $NaBH_4$. It was demonstrated that the combination of $C_{12}C_6C_{12}Br_2$ and Au^{I} plays a key role in regulating the structure of the hollow precursors not only because $C_{12}C_6C_{12}Br_2$ has a stronger aggregation ability in comparison with its single chain counterpart but also because the electrostatic repulsion between head groups of $C_{12}C_6C_{12}Br_2$ is greatly weakened after Au^{III} is converted to Au^{I}, which is in favor of the construction of vesicles, capsule-like, and tube-like aggregates. Compared with solid Au nanospheres, the resultant hollow nanostructures exhibit enhanced electrocatalytic activities in methanol oxidation, following the order of elongated nanocapsule > nanocapsule > nanosphere. Benefiting from balanced interactions between the gemini surfactant and Au^{I}, this soft-template method may present a facile and versatile approach for the controlled synthesis of Au nanostructures potentially useful for fuel cells and other Au nanodevices.

KEYWORDS: hollow Au nanostructures, stepwise reduction, gemini surfactant, template, electrocatalytic oxidation
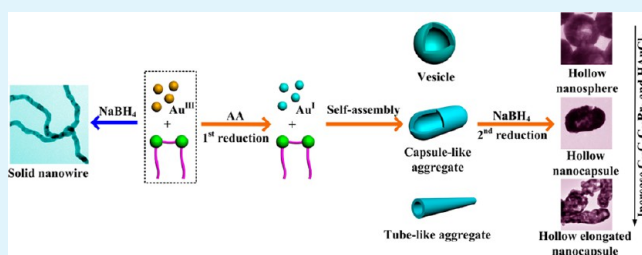
1. INTRODUCTION

Noble metal nanostructures have many fascinating properties depending on their morphologies; hence manipulating morphology is one of the efficient approaches to achieving nanostructures with desired physical and chemical properties for different applications.[1−3] Wide investigations have demonstrated that metallic hollow nanostructures are superior to solid nanostructure in photothermal ablation (PTA) therapy,[4−8] drug delivery,[9] chemical- or bio-sensor,[10,11] near-infrared optical device,[12] surface enhanced Raman scattering (SERS),[13,14] and enhanced catalytic property[15−17] due to their high surface area-to-volume ratios. For instance, Liang et al.[18] found that hollow Pt nanospheres were twice as active in electrocatalytic methanol oxidation as solid Pt nanoparticles of approximately the same size. Kim et al.[19] reported that hollow Pd spheres showed good catalytic activities in Suzuki cross-coupling reactions and could be reused for many times without a loss of catalytic activity.

Currently, metallic hollow nanostructures are mainly fabricated by using a hard template strategy: (a) applying metal (more active) nanoparticles as a template to generate another kind of metal (less active) hollow nanostructure through a galvanic replacement reaction[11,15,18,20−22] and (b) applying anodized aluminum oxide (AAO) or silica/polymeric

spheres as templates through chemical/electrochemical deposition.[10,19,23,24] Benefitting from these methods, various hollow nanostructures, such as rings,[25] shells,[26] cages,[20,21] and tubes,[22] have been constructed. For example, Xia and co-workers[21] demonstrated a simple method to obtain Au−Ag nanocages containing hollow interiors and controllable pores at all corners by using a galvanic replacement reaction between Ag nanocubes and aqueous $HAuCl_4$. However, hard template strategy has some shortcomings including low efficiency, high cost, and the complicated preparation and removal process for templates, which limit its practical application.[27] A soft template method taking advantage of various surfactant aggregates may provide a feasible way to overcome these disadvantages. Zhang et al.[28] reported a one-step facile synthesis of hollow Ag spheres using complex micelles of poly(ethylene oxide)-*block*-poly-(methacrylic acid)-sodium dodecyl sulfate (PEO-*b*-PMAA-SDS) as templates. Kijima et al.[29] reported the construction of Pt, Pd, and Ag nanotubes with a lyotropic liquid crystal template of mixed surfactants. Nevertheless, up to now, the available surfactant templates for colloidal synthesis of metal

hollow nanostructures are still rather limited. One of the possible reasons is that surfactant aggregates are a class of dynamic molecular assemblies and may lose their structure in the complex nucleation and growth of metal nanoparticles.[30,31] Recently, we found the aggregates of gemini surfactant-HAuCl$_4$ complexes were stable enough to be the templates for one-dimensional Au nanostructures because of the strong aggregation ability of gemini surfactants.[30] When surfactants were previously applied in the synthesis of Au nanostructures, Au^{III} was normally used rather than Au^I. However, due to their different valences, Au^{III} and Au^I should display different binding abilities with charged head groups of surfactants and lead to complexes of different structures and morphologies. Moreover, both theoretical and experimental methods have proved that Au^I can form Au^I complexes through non-bonding contacts, i.e., aurophilic interaction.[32] The aurophilic interaction could be applied to build supramolecular architectures such as rings and chains that have potential applications in template synthesis of Au nanostructures.[33−35] Accordingly, it is desired to explore the combination of gemini surfactants and Au^I species in the synthesis of Au nanostructures.

Herein, by using a stepwise reduction method, a facile soft-template approach has been developed with a cationic gemini surfactant hexamethylene-1,6-bis(dodecyl dimethylammonium bromide) (C$_{12}$C$_6$C$_{12}$Br$_2$), and Au^I species and various hollow Au nanostructures including nanospheres, nanocapsules, and elongated nanocapsules have been obtained. Au^I was in situ generated by the reduction of Au^{III} by using a mild reductant AA, while the Au nanostructures (Au^0) were fabricated through the reduction of Au^I by a strong reductant NaBH$_4$. Effects of the total concentration of C$_{12}$C$_6$C$_{12}$Br$_2$ and HAuCl$_4$ and the Au^I/Au^{III} ratio have been investigated, and the possible mechanism has been discussed. Finally, the catalytic activity of the hollow Au nanomaterials in methanol electro-oxidation was evaluated by cyclic voltammetry, and the hollow nanostructures exhibited high activity.

2. MATERIALS AND METHODS

Materials. Chloroauric acid (HAuCl$_4$·4H$_2$O) was purchased from Shenyang Jinke Reagents Company. Ascorbic acid (AA) and sodium borohydride (NaBH$_4$) of analytical grade were obtained from Beijing Chemical Reagents Plant. Gemini surfactant hexamethylene-1,6-bis(dodecyl dimethylammonium bromide) (C$_{12}$C$_6$C$_{12}$Br$_2$) was synthesized as reported in the literature[36] and was used after repeated recrystallization from ethanol. Ultrapure water (Milli-Q, 18.2 MΩ cm) was used to prepare all the solutions.

Synthesis and Characterization of Au Hollow Nanostructures. As a typical procedure, 80 μL of 50 mM C$_{12}$C$_6$C$_{12}$Br$_2$ solution, 100 μL of 20 mM HAuCl$_4$ aqueous solution, and 40 μL of 50 mM AA aqueous solution were added sequentially into 10 mL of water and vortexed. After that, the mixed solution was held at 25 °C for 6 h. After 6 h of aging, 120 μL of ice-cold freshly prepared NaBH$_4$ (100 mM) was rapidly injected into the above mixture with stirring for 1 min, and then the reaction mixture was kept at 25 °C under static conditions for 2 h. The products were collected by centrifugation and washed several times with water and re-suspended in water for further characterizations.

The Au nanostructures were characterized by UV−vis spectroscopy (Shimadzu, UV-1601), scanning electron microscopy (SEM, Hitachi S4800 or S4300, 10 kV), transmission electron microscopy (TEM, JEM-1011, 100 kV, or JEM-2100F, 200 kV) and X-ray diffraction (XRD, Rigaku D/max-2500, Cu Kα radiation, 40 kV, 200 mA). SEM and TEM samples were prepared by placing one drop of the aqueous dispersion of gold product on a silicon wafer or a carbon-coated copper grid, allowing water to evaporate at ambient temperature. For the XRD measurements, several drops of gold product aqueous

dispersion were put on a glass slide, followed by drying naturally in the air.

Characterization of C$_{12}$C$_6$C$_{12}$Br$_2$ Aggregates. The C$_{12}$C$_6$C$_{12}$Br$_2$ aggregates formed after the first reduction of AA were characterized by TEM (JEM-1011, 100 kV). To avoid obvious changes in the aggregates during the sample drying process, the TEM samples were prepared by placing a drop of the AA-reduced solution on a carbon-coated copper grid and allowed to settle for several minutes, and then the excess solution was blotted away by filter paper.

Electrochemical Oxidation of Methanol with Hollow Au Nanostructures. An electrochemical workstation (CV, CHI660B, Chenhua, China) with a three-electrode cell was used to perform electrocatalytic methanol oxidation. A Ag/AgCl electrode (KCl-saturated) and a platinum wire were used as a reference electrode and auxiliary electrode, respectively. The working electrode was a glassy carbon electrode (4 mm) modified with hollow Au nanostructures. The glassy carbon electrode was first polished with 0.05 μm alumina powders and then washed in water and ethanol by ultrasonic treatment. Afterwards, a 10 μL suspension of 0.1 g/L of Au hollow nanostructures was dropped onto the glassy carbon electrode surface and dried under an infrared lamp. Finally, 4 μL of 0.5 wt % Nafion alcohol solution was cast on the surface of the electrode and dried naturally in the air. For electrocatalytic oxidation of methanol, the electrolyte was an aqueous solution of 0.1 M KOH and 1 M methanol. For comparison purposes, solid Au nanospheres 100 nm in diameter (Figure S1 in Supporting Information) were synthesized using a seed-mediated method and then used for electrochemical experiments. Before each measurement, the solution was bubbled with nitrogen for 30 min to remove dissolved oxygen gas.

3. RESULTS AND DISCUSSION

Synthesis and Characterization of Hollow Au Nanostructures. Au nanostructures were synthesized through a stepwise reduction of HAuCl$_4$, first by a weak reductant AA and then a strong reductant NaBH$_4$ in the presence of C$_{12}$C$_6$C$_{12}$Br$_2$. In all the syntheses, the molar ratio of the C$_{12}$C$_6$C$_{12}$Br$_2$/HAuCl$_4$/AA/NaBH$_4$ was fixed at 2:1:1:6. Figure 1 presents the
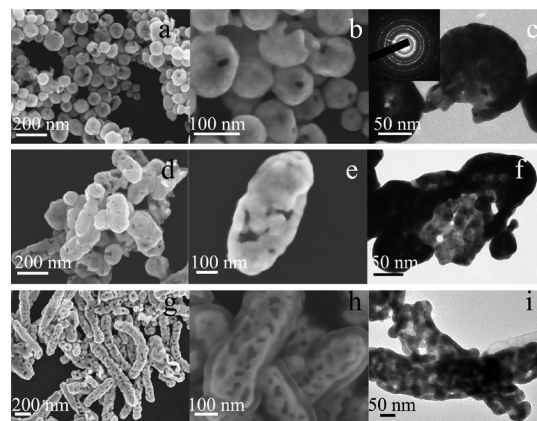

Figure 1. SEM and TEM images of the Au nanostructures obtained by using a stepwise reduction at different total concentrations (C_T) of C$_{12}$C$_6$C$_{12}$Br$_2$ and HAuCl$_4$: 0.6 mM (a−c), 1.2 mM (d−f), 1.8 mM (g−i). The molar ratio of the C$_{12}$C$_6$C$_{12}$Br$_2$/HAuCl$_4$/AA/NaBH$_4$ is 2:1:1:6. The inset in c shows the related SAED pattern.

SEM and TEM images of the different Au nanostructures obtained with an increase of the total concentration of C$_{12}$C$_6$C$_{12}$Br$_2$ and HAuCl$_4$ (C_T). It was found that the C_T greatly influenced the morphology of the gold products. At C_T = 0.6 mM, the Au products are nanospheres with a diameter from 30 to 150 nm (Figure 1a), and some nanospheres have a hole on their shells (Figure 1b), which clearly indicates that the

nanospheres are hollow. The TEM image of Figure 1c presents a typical hollow nanosphere with opening-shell structure, the high contrast of which suggests that the shell is thick. The shell thickness from the holes of the shells in the SEM images is from 16.9 nm to 28.5 nm, and the average thickness value is about 21.9 nm. The electron diffraction (ED) pattern (the inset of Figure 1c) of the nanosphere exhibits sharp rings that can be indexed as polycrystalline face-centered-cubic (fcc) gold. The polycrystalline structure can be further confirmed by the HRTEM image (Figure S2 in Supporting Information) taken from the surface of an individual hollow Au nanosphere. Two types of lattice planes with d spaces of 0.23 and 0.20 nm exist in the image, which can be attributed to the (111) and (200) lattice spaces. The lattice fringes in different regions possess different orientations, suggesting that the hollow nanosphere is composed of small nanoparticles arranged in different directions. When C_T increases to 1.2 mM, the Au products transform into nanocapsules 150−200 nm in diameter and hundreds of nanometers in length (Figure 1d−f). With further increasing C_T to 1.8 mM, the Au nanocapsules are still 150−200 nm in diameter while their length is elongated to several micrometers (Figure 1g−i). The average shell thicknesses of nanocapsules and elongated nanocapsules are 28.7 nm and 21.5 nm, respectively. The HRTEM images of the nanocapsules and elongated nanocapsules (Figure S2) indicate that these nanostructures are also polycrystalline. The XRD patterns of the hollow Au nanospheres, nanocapsules, and elongated nanocapsules show several reflections characteristic of fcc gold (JCPDS No. 04-0784), indicating that the as-prepared hollow nanostructures are pure gold crystals (Figure 2).
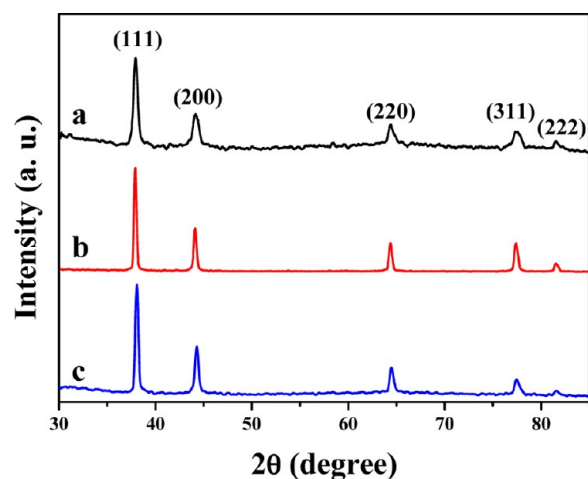

Figure 2. XRD pattern of the hollow Au nanospheres (a), nanocapsules (b), and elongated nanocapsules (c).

Obviously, the final products elongate in one dimension with the increase of C_T. Moreover, compared with the hollow nanospheres, nanocapsules and elongated nanocapsules have more holes on their shells.

Metal hollow nanostructures are a class of nanoparticles with intriguing surface plasmon resonance (SPR) properties determined by their geometrical parameters such as shell thickness, cavity size, and morphology.[37,38] Hence, the SPR absorption properties of the hollow Au nanospheres, nano-capsules, and elongated nanocapsules were studied as shown in Figure 3. As can be seen, hollow Au nanospheres show a strong plasmon resonance peak around 626 nm (curve a). For the
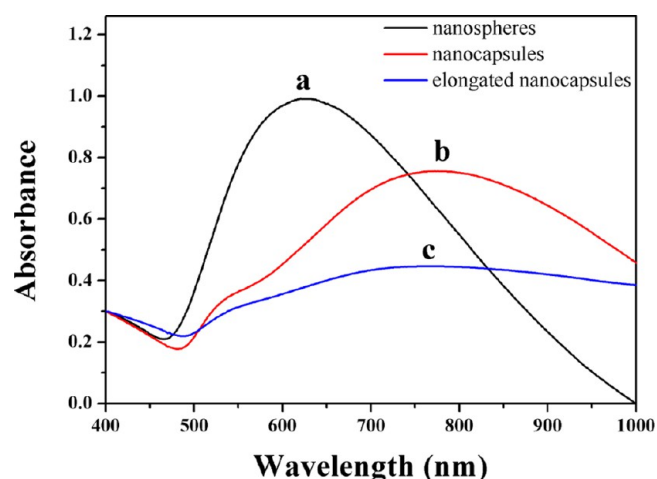

Figure 3. UV−vis spectra of the as-prepared hollow Au nanospheres (a), nanocapsules (b), and elongated nanocapsules (c).

nanocapsules, the strong absorption peak red shifts to ∼780 nm; meanwhile, a weak resonance can be observed at ∼530 nm in the spectrum (curve b). These two resonances can be taken as the longitudinal plasmon mode and transverse plasmon mode, respectively, which is similar to the SPR properties of hollow Au nanorices reported by Wang et al.[39] Interestingly, for the elongated nanocapsules, the transverse resonance shows no obvious change, but the longitudinal resonance displays a broad adsorption from the visible to near infrared region due to the elongation of this nanostructure (curve c).

Influence of Stepwise Reduction. As mentioned above, both AA and $NaBH_4$ were used as reductants in the synthesis of Au nanostructures. The reduction processes are presented in Scheme 1. When mild reductant AA was added into a mixed

Scheme 1. Stepwise Reduction of Au^{III} to Au^{I} by AA and Au^{I} to Au^{0} by $NaBH_4$

$$Au^{I} + BH_4^- + 3H_2O \longrightarrow Au^0 + B(OH)_3 + 3.5H_2 \qquad (2)$$
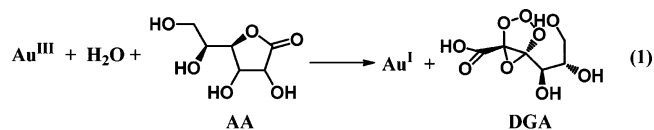
solution of $HAuCl_4$ and $C_{12}C_6C_{12}Br_2$ at a 1:1 AA/$HAuCl_4$ molar ratio, the color of the solution changed from dark yellow to colorless, indicating the reduction of Au^{III} to Au^{I}.[40] According to equation 1,[41] one weak reductant AA molecule can reduce one Au^{III} ion into a Au^{I} ion. The reduction of Au^{III} to Au^{I} was further checked by UV−vis spectroscopy (Figure S3 in the Supporting Information). The spectrum of the mixed solution before AA reduction presents two absorption peaks ascribed to the charge transfer and d−d transition bands of $HAuCl_4$. In contrast, after AA reduction, both of the bands disappear, and no obvious absorption peaks can be observed, indicating the reduction of Au^{III} to Au^{I}. When strong reductant $NaBH_4$ was introduced, according to equation 2, the Au^{I} was reduced to Au^0, forming the final Au products. It was found that $NaBH_4$ was essential in the second step reduction. When more than 1 equivalent (corresponding to $HAuCl_4$) of AA was used to replace $NaBH_4$, branched Au nanostructures (Figure 4) were obtained rather than the hollow nanostructures, suggesting that
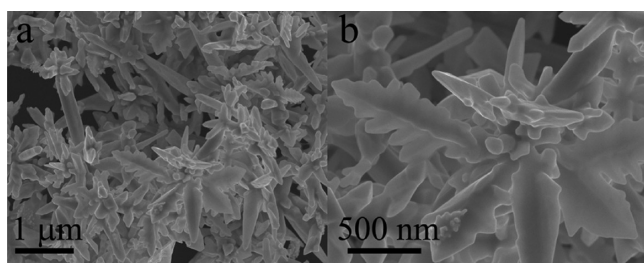
Figure 4. SEM images of Au nanostructures obtained through replacing NaBH$_4$ with excess AA in the second reduction step.

stepwise reduction benefiting from the ingenious combination of weak and strong reductants is a key for the formation of the hollow nanostructures. The Au^I-mediated stepwise reduction procedure was also testified to by using another reductant combination of Na$_2$SO$_3$ with NaBH$_4$, where Na$_2$SO$_3$ played the role of a weak reductant and reduced Au^{III} to Au^I, and NaBH$_4$ acted as the strong reductant. The resulting Au products were hollow nanotubes and nanospheres (Figure S4).

Moreover, the pH value of the reaction solution also affects the formation of hollow Au nanostructures. The pH effects were examined as follows. The initial pH value of 0.4 mM C$_{12}$C$_6$C$_{12}$Br$_2$ and 0.2 mM HAuCl$_4$ was about 3.2. Then the pH was adjusted to 2, 7, and 10 by using 0.5 M HCl or 0.5 M NaOH. When 1 equivalent of AA was rapidly injected into the mixed solutions, the color of the reaction solution changed from light pale to purple and wine red, respectively (Figure S5), with the increase of the pH value from 2 to 7 and 10. The corresponding UV−vis spectra are shown in Figure S5. Taking the case at pH = 7 as an example, besides the charge transfer and d−d transition adsorptions of Au^{III}, a new peak around 550 arises, which should be from the formation of a metallic Au nanostructure. These results indicate that partial Au^{III} ions have been reduced to Au^0 without going though the period of Au^I. Therefore the pH value alters the processes of the formation of the Au nanostructures.

Influence of Au^I/Au^{III} Ratio. In order to clarify the role of Au species in the formation of the hollow nanostructures, effects of the Au^I/Au^{III} ratio on the Au products were studied. In the studies, the Au^I/Au^{III} ratio was modulated by adjusting the amount of the reductant AA according to Scheme 1, while the concentration of C$_{12}$C$_6$C$_{12}$Br$_2$, HAuCl$_4$, and NaBH$_4$ was fixed at 0.4, 0.2, and 1.2 mM, respectively. Because 0, 0.02, 0.10, and 0.16 mM AA were separately used in the first reduction step, the corresponding Au^I/Au^{III} ratios in the four reaction systems were about 0, 1:4, 1:1, and 4:1, estimated from the reactions in Scheme 1. Figure 5 shows the influence of the Au^I/Au^{III} ratio on the morphology of the final Au products. When AA was not used but only NaBH$_4$ was used, Au^{III} was directly reduced into Au^0, i.e., Au^I/Au^{III} = 0. The final product was solid Au nanowires ∼30 nm in diameter and several micrometers in length (Figure 5a). A close-up image of the nanowire (Figure S6) further confirms that the obtained nanowires are in a solid structure. When the Au^I/Au^{III} ratio became 1:4 in the synthesis process, the Au product changed into short nanowires with several hundreds of nanometers together with a small amount of nanospheres (Figure 5b). While the Au^I/Au^{III} ratio changes to 1:1, the Au product was hollow nanospheres ∼50 nm in diameter accompanied with a very small amount of short nanowires (Figure 5c). Further increasing the Au^I/Au^{III} ratio to 4:1, the Au product was uniform hollow Au nanospheres with a

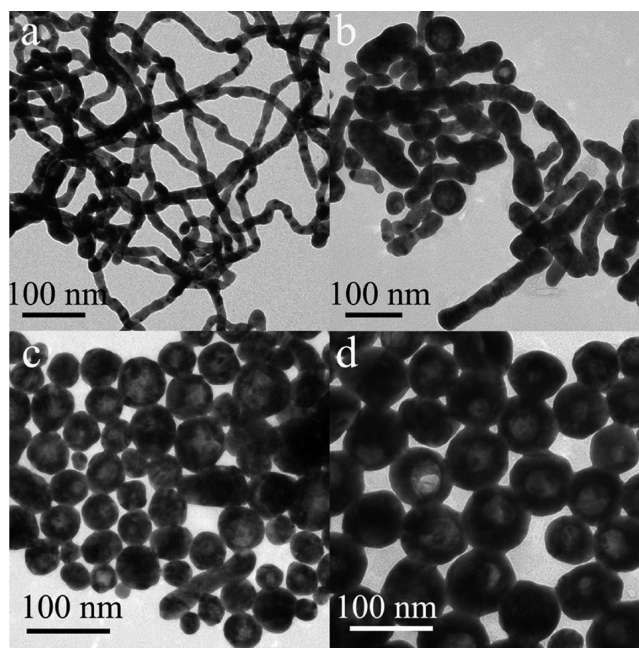**Figure 5.** TEM images of the Au nanostructures obtained at different Au^I/Au^{III} ratios: 0 (a), 1:4 (b), 1:1 (c), and 4:1 (d). [C$_{12}$C$_6$C$_{12}$Br$_2$] = 0.4 mM, [HAuCl$_4$] = 0.2 mM, [NaBH$_4$] = 1.2 mM.

diameter of ∼80 nm (Figure 5d). Obviously, only when the Au^I/Au^{III} ratio is large enough can the hollow Au nanostructures be generated. That is to say, the Au^{III} favors the formation of solid nanostructures, while the Au^I facilitates the generation of hollow nanostructures. Moreover, the increase of the Au^I/Au^{III} ratio decreases the length of the Au nanostructures while enlarging their diameter. In brief, this finding indicates that the Au^I/Au^{III} ratio is one of the key determining factors for the nanostructure and morphology of final Au products in the surfactant-assisted synthesis.

Influence of C$_{12}$C$_6$C$_{12}$Br$_2$. To understand the role of the gemini surfactant C$_{12}$C$_6$C$_{12}$Br$_2$ with two quaternary ammonium head groups and two alkyl chains in the formation of the hollow Au nanostructures, the corresponding cationic single chain surfactant dodecyltrimethylammonium bromide (DTAB) was used instead of C$_{12}$C$_6$C$_{12}$Br$_2$ to synthesize Au nanostructures under the same experimental conditions. Solid Au products were observed rather than the hollow nanostructures (data not shown). This result indicates that the gemini surfactant plays an important role in the formation of the hollow Au nanostructures.

In the Au synthesis processes in the presence of C$_{12}$C$_6$C$_{12}$Br$_2$, after the first reduction step by AA, it was observed that the color of the solutions containing C$_{12}$C$_6$C$_{12}$Br$_2$ and Au^I gradually changed from colorless to milk white with the time. This optic phenomenon suggests the formation of large aggregates in the mixed solutions. Figure 6 presents the TEM images of the C$_{12}$C$_6$C$_{12}$Br$_2$−Au^I aggregates formed after the first AA reduction step at different total concentrations of C$_{12}$C$_6$C$_{12}$Br$_2$ and HAuCl$_4$ (C_T). In all the solutions, the molar ratio of C$_{12}$C$_6$C$_{12}$Br$_2$/HAuCl$_4$/AA is 2:1:1. At C_T = 0.6 mM, the mixture formed spherical aggregates (Figure 6a). The spherical aggregates are composed of many small nanoparticles, which are Au nanoparticles after the in situ reduction of Au^I under the irradiation of the TEM electron beam. The number density of the Au nanoparticles around the edge of the

5712

dx.doi.org/10.1021/am4011226 | ACS Appl. Mater. Interfaces 2013, 5, 5709−5716
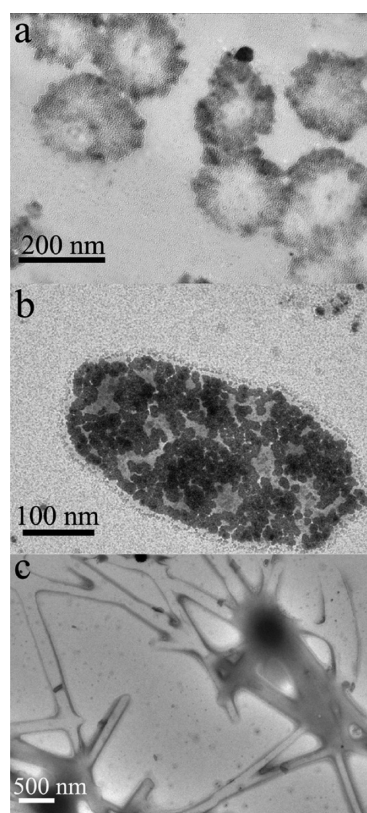
Figure 6. TEM images of the $C_{12}C_6C_{12}Br_2-Au^I$ aggregates formed after the first AA reduction step at different total concentrations of $C_{12}C_6C_{12}Br_2$ and $HAuCl_4$ (C_T): 0.6 mM (a), 1.2 mM (b), and 1.8 mM (c).

aggregates is larger than that inside the aggregates, implying that the Au species are mainly arranged at the outlayer of the spherical aggregates. Subsequently, with the increase of the C_T to 1.2 mM and 1.8 mM, the mixture aggregates are elongated into capsule-like (Figure 6b) and tube-like structures (Figure 6c). Comparing these images with those in Figure 1, apparently, the morphologies of the final Au products after the reduction by $NaBH_4$ closely correlate with the morphologies of the $C_{12}C_6C_{12}Br_2-Au^I$ aggregates formed in the AA-reduced mixtures. Consequently, the $C_{12}C_6C_{12}Br_2-Au^I$ aggre-

gates served as the templates for the formation of the hollow Au nanostructures.

As mentioned above, the nanocapsules and elongated nanocapsules have more holes on their shells than hollow nanospheres. The holes on the shell of gold nanostructures may relate with the participation of Au ions in the templates in the formation of nearby crystalline Au. Besides, H_2 gas was produced during the $NaBH_4$ reduction process, and the release of gas should be another important factor in causing holes in the resultant Au nanostructures. For the nanocapsules and elongated nanocapsules, the used concentrations of Au^I ions and $NaBH_4$ were larger than those of nanospheres, leading to more strong reduction and gas release. The significant increase of the amount of H_2 generated more holes on the nanocapsules.

Possible Formation Mechanism of Hollow Au Nanostructures. On the basis of the above results and discussions, the possible formation mechanism of the Au nanostructures is suggested as follows. Figure 7 summarizes the formation processes of the hollow nanostructures via the stepwise reduction route. First, Au^{III} is reduced to Au^I by adding a mild reductant AA, and then the gemini surfactant and Au^I forms spherical, capsule-like, and tube-like aggregates, depending on the total concentration of $C_{12}C_6C_{12}Br_2$ and $HAuCl_4$. Finally the spherical, capsule-like, and tube-like aggregates are reduced by a strong reductant, $NaBH_4$, yielding hollow Au nanospheres, nanocapsules, and elongated nanocapsules, respectively.

The first reduction of $Au^{III} \rightarrow Au^I$ is one of the key steps. Previously we found that without Au^I, $C_{12}C_6C_{12}Br_2$ and Au^{III} formed worm-like micelles and further associated into fibrillar aggregates,[30] which performed as the templates leading to solid Au nanowires (Figure 5a). With the appearance of Au^I, the $C_{12}C_6C_{12}Br_2/Au^I$ aggregates change significantly. As is well-known, ionic surfactant molecules can form vesicles very often upon binding with oppositely charged ions. The head groups of surfactants bind with oppositely charged ions, leading to the formation of enclosed bilayers of amphiphilic molecules, which is the feature structure of vesicles. Figure 6a shows that Au species mainly existed on the outside of the spherical aggregates, so the spherical aggregates observed may be the vesicles formed by Au^I and the gemini surfactant. These results indicate that the role of Au^{III} and Au^I on the aggregation behavior of the gemini surfactant is quite different. Normally self-assembling structures of surfactants are controlled by the
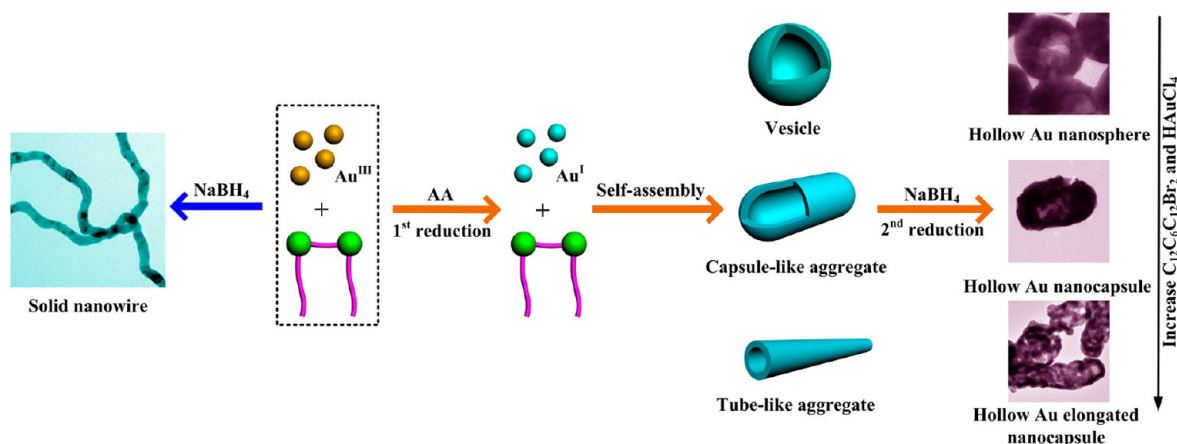

Figure 7. The formation processes of the hollow Au nanostructures by stepwise reduction based on a combination of AA and $NaBH_4$.

5713

dx.doi.org/10.1021/am4011226 | ACS Appl. Mater. Interfaces 2013, 5, 5709−5716

geometry rule,[42] which is described by the packing parameter P = v/a_0l_c, where v is the volume of the hydrophobic chain, a_0 is the cross sectional area of the hydrophilic head group, and l_c is the length of the hydrophobic chain. All the v, a_0, and l_c values of a surfactant are the average values occupied by the surfactant molecules in aggregates. According to the geometry rule, surfactants self-assemble into worm-like micelles at $1/3 < P \leq 1/2$ or spherical vesicles at $1/2 < P \leq 1$. Binding with oppositely charged ions can lessen the micellar surface charge and decrease the a_0 value by weakening electrostatic repulsion between the head groups and in turn result in the increase of P values.[43−45] Because the valence of Au^{III} is higher than that of Au^I, Au^{III} should affect P more significantly than Au^I. However the present work above indicates that Au^I affects the P value of the gemini surfactant more significantly than Au^{III}. How does this come to be? The gemini surfactant $C_{12}C_6C_{12}Br_2$ has Br$^-$ as its counterion, and the HAuCl$_4$ molecules in the reaction solution contain Cl$^-$. Au^{III} can adopt dsp^2 hybridization to form $[AuL_4]^-$ (L = Br, Cl) with Br$^-$ and Cl$^-$, whereas Au^I can adopt sp hybridization to form $[AuL_2]^-$. The $[AuL_4]^-$ and $[AuL_2]^-$ ions are in quadractic planar and linear shapes, respectively. The $[AuL_4]^-$ ions may have a larger steric hindrance than the $[AuL_2]^-$ ions while interacting with the quaternary ammonium cations of the gemini surfactant. Previously, Pérez-Juste and coworkers[45] found that $[AuBr_2]^-$ formed more stable complexes with cetyltrimethylammonium bromide (CTAB) than $[AuBr_4]^-$. This is consistent with the present result. Herein, the stronger binding of the cationic head groups of $C_{12}C_6C_{12}Br_2$ with Au^I as $[AuL_2]^-$ greatly weakens the electrostatic repulsion among the head groups of $C_{12}C_6C_{12}Br_2$. Moreover, the Au^I/$C_{12}C_6C_{12}Br_2$ complexes can be further stabilized by the aurophilic interactions of Au^I. The aurophilic binding energy is comparable to that of a hydrogen bond,[47,48] which may provide an additional driving force to lower electrostatic repulsion of the surfactant head groups. As a result, to a larger extent Au^I lessens the head group area of $C_{12}C_6C_{12}Br_2$, leading to a smaller a_0 and a lager P value. Thus, $C_{12}C_6C_{12}Br_2$ tends to form vesicles upon the binding with Au^I while forming wormlike micelles with Au^{III}. If adjusting the Au^I/Au^{III} ratio, the surfactant aggregates with gold ions will change in between these two kinds of aggregates, as presented in Figure S7 of Supporting Information. This is why different Au nanostructures were obtained when the Au^I/Au^{III} ratio was adjusted. This indicates that Au^I ions play a more significant effect on the aggregation behavior of $C_{12}C_6C_{12}Br_2$ because of its different hybridization state from Au^{III} and the aurophilic attraction between Au^I species. Thus, the Au^I/Au^{III} ratio alters the self-assembling process of $C_{12}C_6C_{12}Br_2$, yielding uniform hollow Au nanostructures with different morphologies.

Besides, using a strong reductant (such as NaBH$_4$) in the second reduction step is necessary; otherwise hollow nanostructures could not be obtained. As illustrated in Figure 4, when NaBH$_4$ was replaced by excess AA in the second reduction step, branched Au nanostructures were obtained rather than the hollow nanostructures. Normally surfactant aggregates are a class of dynamic molecular assemblies which exist in a dynamic equilibrium with monomers. If the second reduction rate is too low, the surfactant aggregates will change gradually and cannot act as ideal templates. That is to say, the template mechanism cannot work well at a lower reduction rate.

As we mentioned in the above text, gemini surfactant $C_{12}C_6C_{12}Br_2$ is another prerequisite for the formation of the hollow nanostructures. The single chain surfactant DTAB failed to do this as we observed. Likewise, Jana[49] found that the rod-like CTAB micelles could not preserve their shapes during the growth of Au nanocrystals. Compared with conventional single chain surfactants, gemini surfactants display a much stronger aggregation ability.[50−53] The strong aggregation ability makes them an ideal template agent for the Au nanostructures as proved previously.[30,54,55] The stable and compact aggregates of gemini surfactants can keep their morphologies in the final Au products. Moreover, the gemini surfactant has one more charged head group than DTAB; thus the gemini surfactant molecules can efficiently attract Au ions to be concentrated at their head group areas and then assemble into various hollow aggregates. This is the most possible reason for the formation of hollow nanostructures in the final Au product.

Another important phenomenon is that with the increase of C_T, the aggregates of $C_{12}C_6C_{12}Br_2$ with the mixture of Au^I and Au^{III} transformed from spherical to capsule-like and further to tube-like. Increasing C_T enhances hydrophobic interaction between the $C_{12}C_6C_{12}Br_2$ molecules, just as most of surfactants do.[45,56,57] Meanwhile, the ionization degree of the $C_{12}C_6C_{12}Br_2$ head groups also decreases with the increase of C_T,[58] which means more counterions exist in the head group domain of the aggregates, weakening the electrostatic repulsion between the head groups and thus further promoting the P value. These variations will lead to the larger and energy favorable aggregates with a lower curvature in one dimension, as with the capsule-like and tube-like aggregates observed above. Accordingly, the spherical, capsule-like, and tube-like aggregates result in the final hollow Au nanostructures with the similar shapes, i.e., nanosphere, nanocapsule, and elongated nanocapsule.

The above discussion is based on packing parameter P determined by the final balances of various intermolecular interactions. For a surfactant, P is not a constant. It changes with the variations of aggregates. It is affected by the hydrophobic chain length, the structure of the head group, solvent, temperature, ionic strength, and so on. The binding of Au ions with the surfactant head groups significantly reduces the electrostatic repulsion between the head groups of different surfactant molecules and in turn brings in a more significant increase in P. It is well known that the spacer length of the gemini surfactant also greatly affects its P value.[50,52,53] Shortening the spacer length of the gemini surfactant will decrease the a_0 and thus increase the P value, showing a similar effect on P to the binding of Au ions with the surfactant head groups. So the gemini surfactants with a shorter spacer can also be used in the formation of the hollow Au nanostructures. As expected, hollow nanostructures were also obtained in the $C_{12}C_2C_{12}Br_2$ system with a short spacer length.

Methanol Electrocatalytic Oxidation. Normally metal hollow nanostructures can exhibit high catalytic activity because of large surface area. So methanol electrocatalytic oxidation was chosen as an example to test the electrocatalytic activities of the prepared hollow Au nanostructures. The hollow Au nanospheres, nanocapsules, and elongated nanocapsules were deposited onto the glassy carbon electrodes to modify glassy carbon electrodes, and the electrocatalytic activities toward the oxidation of methanol were investigated by measuring its cyclic voltammograms (CVs) in KOH solutions. For comparison, a glassy carbon electrode modified by solid Au nanospheres ∼100 nm in diameter was also prepared and examined under identical conditions. The loading mass of the hollow Au nanostructures and the solid nanospheres on the electrode

surface was the same. Figure 8 illustrates the CVs recorded from the four Au electrodes in 2.0 M CH$_3$OH solution with 0.1
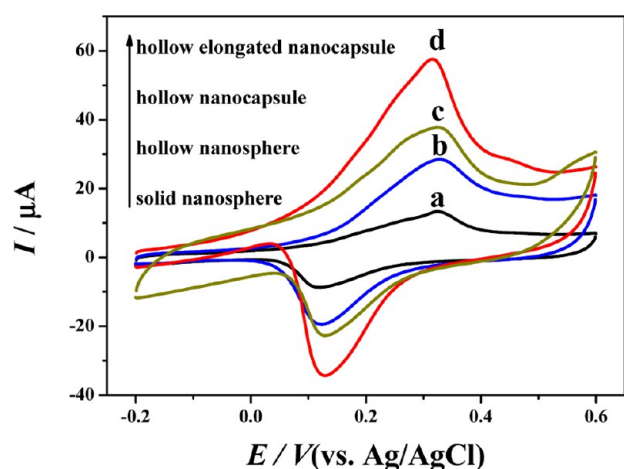

Figure 8. Cyclic voltammograms of Au solid nanosphere (a), hollow nanosphere (b), hollow nanocapsule (c), and hollow elongated nanocapsule (d) in nitrogen-saturated KOH (0.1 M) + CH$_3$OH (2.0 M) solution at a scan rate of 50 mV s^{-1}.

M KOH. The peak current density of the solid Au electrode, hollow nanosphere electrode, hollow nanocapsule electrode, and hollow elongated nanocapsule electrode are 12.31, 28.46, 37.84, and 57.80 μA, respectively, following the order of elongated nanocapsules > nanocapsules > nanosphere > solid Au. The calculated electrochemical active surface areas (ECSA) of the Au solid nanosphere electrode, hollow nanosphere electrode, hollow nanocapsule electrode, and hollow elongated nanocapsule electrode are 0.0962, 0.263, 0.382, and 0.683 cm^2, respectively. The differences in ECSA values and catalytic activities of the Au nanostructures can be interpreted by their morphologies. Because the hollow nanostructures are coreless, the surface area of the hollow nanostructure must be higher than that of the solid nanostructure of the same loading mass. Moreover, the opening-shell structures of hollow nanostructures can provide the interior surface for the catalytic reaction.[16] Thereby both the inner and outer surfaces of the hollow nanostructures can participate in the catalytic reaction. As mentioned above, the hollow elongated nanocapsules have more holes on their shells than those of hollow nanocapsules and nanospheres. Thus the hollow elongated nanocapsules have a larger surface area, providing more electrocatalytic active sites toward the methanol oxidation.

4. CONCLUSIONS

In summary, by using a stepwise reduction method of Au^{III} to Au^I by AA and Au^I to Au^0 by NaBH$_4$ in the presence of cationic gemini surfactant C$_{12}$C$_6$C$_{12}$Br$_2$, hollow Au nanospheres, nanocapsules, and elongated nanocapsules have been successfully fabricated. Systematic studies indicate that Au^I induces C$_{12}$C$_6$C$_{12}$Br$_2$ to self-assemble into vesicles, capsule-like, or tube-like aggregates with increasing the total concentration of C$_{12}$C$_6$C$_{12}$Br$_2$ and HAuCl$_4$, which act as templates for the hollow Au nanostructures. Due to the strong aggregation ability of the gemini surfactant, the templates are stable enough to preserve their shapes during reduction. Au^I is indispensable for the formation of these templates. For instance, the aggregates in the form of vesicles will transform into worm-like micelles if replacing Au^I with Au^{III}, because Au^I can weaken the

electrostatic repulsion between the C$_{12}$C$_6$C$_{12}$Br$_2$ head groups more significantly than Au^{III}. Therefore, the use of C$_{12}$C$_6$C$_{12}$Br$_2$ and the first reduction of Au^{III} to Au^I are the two key factors for the construction of the hollow nanostructures. The as-prepared hollow Au nanostructures display higher electrocatalytic activity towards methanol oxidation. It is anticipated that the Au^I/ gemini surfactant based soft-template method provides a facile and versatile strategy to fabricate Au hollow nanostructures with novel morphologies and properties.

ASSOCIATED CONTENT

Ⓢ Supporting Information

The preparation and SEM images of the solid Au nanospheres, high-resolution TEM image of single Au nanowire synthesized via one-step reduction by NaBH$_4$, photographs and UV−vis spectra of the reaction solution after AA reduction, SEM images of Au nanostructures obtained from the C$_{12}$C$_6$C$_{12}$Br$_2$/HAuCl$_4$/ Na$_2$SO$_3$/NaBH$_4$ system and C$_{12}$C$_2$C$_{12}$Br$_2$/HAuCl$_4$/AA/NaBH$_4$ system, extra TEM images of the C$_{12}$C$_6$C$_{12}$Br$_2$/Au ions aggregates, and cyclic voltammograms of Au products in nitrogen-saturated KOH solution. This material is available free of charge via the Internet at http://pubs.acs.org.

AUTHOR INFORMATION

Corresponding Author

*Tel.: +86-10-82615802. Fax: +86-10-82615802. E-mail: yilinwang@iccas.ac.cn (Y.L.W.), gaomy@iccas.ac.cn (M.Y.G.).

Notes

The authors declare no competing financial interest.

REFERENCES

(1) Burda, C.; Chen, X.; Narayanan, R.; El-Sayed, M. A. *Chem. Rev.* **2005**, *105*, 1025−1102.
(2) Rycenga, M.; Cobley, C. M.; Zeng, J.; Li, W.; Moran, C. H.; Zhang, Q.; Qin, D.; Xia, Y. *Chem. Rev.* **2011**, *111*, 3669−3712.
(3) Zhou, Z. Y.; Tian, N.; Li, J. T.; Broadwell, I.; Sun, S. G. *Chem. Soc. Rev.* **2011**, *40*, 4167−4185.
(4) Zhang, J. Z. *J. Phys. Chem. Lett.* **2010**, *1*, 686−695.
(5) Gobin, A. M.; Lee, M. H.; Halas, N. J.; James, W. D.; Drezek, R. A.; West, J. L. *Nano Lett.* **2007**, *7*, 1929−1934.
(6) Ji, X. J.; Shao, R. P.; Elliott, A. M.; Stafford, R. J.; Esparza-Coss, E.; Bankson, J. A.; Liang, G.; Luo, Z. P.; Park, K.; Markert, J. T.; Li, C. *J. Phys. Chem. C* **2007**, *111*, 6245−6251.
(7) Skrabalak, S. E.; Au, L.; Lu, X. M.; Li, X. D.; Xia, Y. N. *Nanomedicine* **2007**, *2*, 657−668.
(8) Ma, Y.; Liang, X.; Tong, S.; Bao, G.; Ren, Q.; Dai, Z. *Adv. Funct. Mater.* **2013**, *23*, 815−822.
(9) You, J.; Zhang, G.; Li, C. *ACS Nano* **2010**, *4*, 1033−1041.
(10) Zhang, X.; Wang, H.; Bourgeois, L.; Pan, R.; Zhao, D.; Webley, P. A. *J. Mater. Chem.* **2008**, *18*, 463−467.
(11) Wirtz, M.; Yu, S.; Martin, C. R. *Analyst* **2002**, *127*, 871−879.
(12) Bridges, C. R.; DiCarmine, P. M.; Seferos, D. S. *Chem. Mater.* **2012**, *24*, 963−965.
(13) Xie, H. N.; Larmour, I. A.; Smith, W. E.; Faulds, K.; Graham, D. *J. Phys. Chem. C* **2012**, *116*, 8338−8342.
(14) Sanchez-Gaytan, B. L.; Swanglap, P.; Lamkin, T. J.; Hickey, R. J.; Fakhraai, Z.; Link, S.; Park, S. J. *J. Phys. Chem. C* **2012**, *116*, 10318−10324.
(15) Sun, Y. G.; Mayers, B.; Xia, Y. N. *Adv. Mater.* **2003**, *15*, 641−646.

(16) Liu, H.; Qu, J.; Chen, Y.; Li, J.; Ye, F.; Lee, J. Y.; Yang, J. *J. Am. Chem. Soc.* **2012**, *134*, 11602−11610.

(17) Mahmoud, M. A.; Saira, F.; El-Sayed, M. A. *Nano Lett.* **2010**, *10*, 3764−3769.

(18) Liang, H. P.; Zhang, H. M.; Hu, J. S.; Guo, Y. G.; Wan, L. J.; Bai, C. L. *Angew. Chem. Int. Ed.* **2004**, *43*, 1540−1543.

(19) Kim, S. W.; Kim, M.; Lee, W. Y.; Hyeon, T. *J. Am. Chem. Soc.* **2002**, *124*, 7642−7643.

(20) Chen, J.; Saeki, F.; Wiley, B. J.; Cang, H.; Cobb, J. M.; Li, Z.; Au, L.; Zhang, H.; Kimmey, M. B.; Li, X.; Xia, Y. *Nano Lett.* **2005**, *5*, 473−477.

(21) Chen, J.; McLellan, J. M.; Siekkinen, A.; Xiong, Y.; Li, Z.; Xia, Y. *J. Am. Chem. Soc.* **2006**, *128*, 14776−14777.

(22) Sun, Y.; Mayers, B.; Herricks, T.; Xia, Y. *Nano Lett.* **2003**, *3*, 955−1000.

(23) Wirtz, M.; Martin, C. R. *Adv. Mater.* **2005**, *15*, 455−458.

(24) Jankiewicza, B. J.; Jamiolab, D.; Chomab, J.; Jaroniecc, M. *Adv. Colloid Interface Sci.* **2012**, *170*, 28−47.

(25) Liusman, C.; Li, S.; Chen, X.; Wei, W.; Zhang, H.; Schatz, G. C.; Boey, F.; Mirkin, C. A. *ACS Nano* **2010**, *4*, 7676−7682.

(26) Mirin, N. A.; Ali, A. T.; Nordlander, P.; Halas, N. J. *ACS Nano* **2010**, *4*, 2701−2712.

(27) Lou, X. W.; Archer, L. A.; Yang, Z. *Adv. Mater.* **2008**, *20*, 3987−4019.

(28) Zhang, D.; Qi, L.; Ma, J.; Cheng, H. *Adv. Mater.* **2002**, *14*, 1499−1502.

(29) Kijima, T.; Yoshimura, T.; Uota, M.; Ikeda, T.; Fujikawa, D.; Mouri, S.; Uoyama, S. *Angew. Chem. Int. Ed.* **2004**, *43*, 228−232.

(30) Wang, W.; Han, Y.; Gao, M.; Wang, Y. L. *J. Nanopart. Res.* **2013**, *15*, 1380.

(31) Qiao, Y.; Wang, Y.; Yang, Z.; Lin, Y.; Huang, J. *Chem. Mater.* **2011**, *23*, 1182−1187.

(32) Pyykkö, P. *Angew. Chem. Int. Ed.* **2004**, *43*, 4412−4456.

(33) Gomez, S.; Philippot, K.; Collière, V.; Chaudret, B.; Senocq, F.; Lecante, P. *Chem. Commun.* **2000**, 1945−1946.

(34) Simpson, C. A.; Farrow, C. L.; Tian, P.; Billinge, S. J. L.; Huffman, B. J.; Harkness, K. M.; Cliffel, D. E. *Inorg. Chem.* **2010**, *49*, 10858−10866.

(35) Lu, X.; Yavuz, M S.; Tuan, H.-Y.; Korgel, B. A.; Xia, Y. *J. Am. Chem. Soc.* **2008**, *130*, 8900−8901.

(36) Zana, R.; Benrraou, M.; Rueff, R. *Langmuir* **1991**, *7*, 1072−1075.

(37) Halas, N. J. *MRS Bull.* **2005**, *30*, 362−367.

(38) Radloff, C.; Halas, N. J. *Nano Lett.* **2004**, *4*, 1323−1327.

(39) Wang, H.; Brandl, D. W.; Le, F.; Nordlander, P.; Halas, N. J. *Nano Lett.* **2006**, *6*, 827−832.

(40) Gao, J.; Bender, C. M.; Murphy, C. J. *Langmuir* **2003**, *19*, 9065−9070.

(41) Wang, L.; Hu, C.; Nemoto, Y.; Tateyama, Y.; Yamauchi, Y. *Cryst. Growth Des.* **2010**, *10*, 3454−3460.

(42) Israelachvili, J. N.; Mitchell, D. J.; Ninham, B. W. *J. Chem. Soc., Faraday Trans. II* **1976**, *72*, 1525−1568.

(43) Yu, D.; Wang, Y.; Zhang, J.; Tian, M.; Han, Y.; Wang, Y. L. *J. Colloid Interface Sci.* **2012**, *381*, 83−88.

(44) Jiang, L.; Wang, K.; Deng, M.; Wang, Y.; Huang, J. *Langmuir* **2008**, *24*, 4600−4606.

(45) Pérez-Juste, J.; Liz-Marzán, L. M.; Carnie, S.; Chan, D. Y. C.; Mulvaney, P. *Adv. Funct. Mater.* **2004**, *14*, 571−579.

(46) Yu, D.; Huang, X.; Deng, M.; Lin, Y.; Jiang, L.; Huang, J.; Wang, Y. L. *J. Phys. Chem. B* **2010**, *114*, 14955−14964.

(47) Pyykkö, P.; Runeberg, N.; Mendizabal, F. *Chem.—Eur. J.* **1997**, *3*, 1451−1457.

(48) Pyykkö, P. *Chem. Rev.* **1997**, *97*, 597−636.

(49) Jana, N. R. *Small* **2005**, *1*, 875−882.

(50) Menger, F. M.; Keiper, J. S. *Angew. Chem., Int. Ed.* **2000**, *39*, 1906−1920.

(51) Han, Y.; Wang, Y. L. *Phys. Chem. Chem. Phys.* **2011**, *13*, 1939−1956.

(52) Zana, R. *Curr. Opin. Colloid Interface Sci.* **1996**, *1*, 566−571.

(53) Zana, R. *J. Colloid Interface Sci.* **2002**, *248*, 203−220.

(54) Esumi, K.; Hara, J.; Aihara, N.; Usui, K.; Torigoe, K. *J. Colloid Interface Sci.* **1998**, *208*, 578−581.

(55) Bakshi, M. S.; Possmayer, F.; Petersen, N. O. *J. Phys. Chem. C* **2008**, *112*, 8259−8265.

(56) Hou, Y.; Han, Y.; Deng, M.; Xiang, J.; Wang, Y. L. *Langmuir* **2010**, *26*, 28−33.

(57) Fan, Y.; Hou, Y.; Xiang, J.; Yu, D.; Wu, C.; Tian, M.; Han, Y.; Wang, Y. L. *Langmuir* **2011**, *27*, 10570−10579.

(58) Kuwamoto, K.; Asakawa, T.; Ohta, A.; Miyagishi, S. *Langmuir* **2005**, *21*, 7691−7695.